A MIMO PLC Random Channel Generator and Capacity Analysis

Fabio Versolatto and Andrea M. Tonello
DIEGM - Università di Udine - Via delle Scienze 208 - 33100 Udine - Italy
phone: +39 0432 558042 - fax: +39 0432 558251 - e-mail: fabio.versolatto@uniud.it, tonello@uniud.it

***Abstract*—We propose a bottom-up power line communication (PLC) channel generator that exploits multi conductor transmission line (MTL) theory combined with a random topology generation algorithm to generate statistically representative in-home multiple-input multiple-output (MIMO) PLC channels. We focus on in-home PLC networks that deploy three conductors and thus provide two different circuits sharing the same return conductor. Therefore, we consider a 2×2 MIMO PLC system. We evaluate the capacity gain achieved by the MIMO configuration w.r.t. the single-input single-output (SISO) case, i.e., when only two wires are used. We further compare the simulated results with the experimental ones presented in the literature, and we show their convergence in statistical terms.**

I. Introduction

In-home power line communications aim to exploit the existent electrical infrastructure to deliver high speed services without the installation of new wires. Although the electrical infrastructure was not designed for high speed communications, it has been gaining interest as a mean to convey information due to its widespread presence and its large number of access points, namely, outlets, where the electrical appliances are connected to. Typically, the electricity is delivered via three conductors, i.e., the phase, the neutral and the protective earth (PE).

State-of-the-art standards in PLC ensure communications up to 200 Mbps by signalling over the phase and the neutral in the 1-30 MHz frequency band [1]. Communications beyond 200 Mbps have been shown to be feasible by extending the bandwidth up to 100 MHz [2]. A further improvement can be achieved exploiting the PE wire. Basically, with three conductors, two different circuits are given and thus a 2×2 MIMO system is defined.

MIMO communications were firstly introduced in wireless, where it has been shown that, without any increase in the transmitted power, a $n \times n$ MIMO scheme could yield a capacity increase that grows linearly with n, the number of transmitter and receiver antennas [3]. In PLC, the first attempt towards MIMO was done in [4] - [5], where space-time and space frequency codes were applied to multiple phase power line networks with uncoupled wires. Later, in [6], the capacity improvement provided by the precoded spatial multiplexing MIMO scheme was also investigated up to 30 MHz in single phase in-home networks. To this aim, a database of MIMO channel transfer functions was collected from an experimental measurement campaign in several houses and flats. More recently, the results of a measurement campaign up to 100 MHz in single phase networks were provided in [7].

In this paper we devise a bottom-up MIMO PLC random channel generator that exploits the multiconductor transmission line (MTL) theory and a statistical topology generator algorithm [8] to provide random MIMO PLC channel responses that are in good agreement with results obtained in measurement campaigns. We focus on single phase in-home networks in the 2-100 MHz frequency band. We investigate the MIMO and the single-input multiple-output (SIMO) configuration, namely, when only one transmitter is present. We also infer the MIMO performance in networks where the neutral and ground wires are short circuited in the main panel, as in the NEC-compliant North American systems.

The paper is organized as follows. In Section II, we provide the theoretical analysis of the three conductor configuration and we derive the MTL extension of the channel transfer function (CTF) computation algorithm that we refer to as voltage ratio approach [9]. In Section III, we describe the topology generation algorithm [8]. Then, in Section IV, we describe the considered channel statistics, and in Section V we show the numerical results. Finally, some conclusions follow.

II. Analysis of the MTL Configuration

In this section, we propose the MTL extension of the voltage ratio approach in [9]. To this aim, we recall the fundamental relations of MTL theory and we exploit them in order to devise an efficient MIMO channel transfer function computation algorithm based on the voltage-ratio approach.

A. Three Conductors Transmission Line Equations

We focus on the three conductor power line installations where the wires can be modelled as parallel good conductors sheathed in a uniform dielectric material and nearby placed. This is the case, for instance, where compact and symmetrical cables are deployed. In symmetrical cables, each wire is independently sheathed and enclosed in a PVC cap, and further the inter-distance between conductors is constant.

Since the transversal dimension of the overall cable structure is relatively small w.r.t. the transmission signal wavelength in the range of frequencies that we consider, i.e., in the lower GHz range, we can make the transverse electromagnetic (TEM) or quasi-TEM mode assumption [10]. It follows that we can use the equivalent per-unit-length (p.u.l.) parameter model to characterize the three-conductors cable. Fig. 1 shows a

978-1-4244-7749-4/11/$26.00 ©2011 IEEE

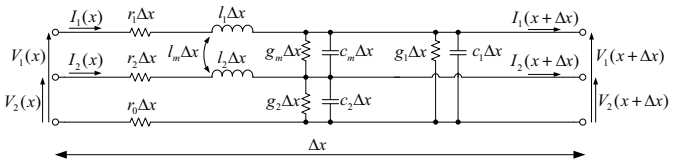

Fig. 1. Equivalent per-unit-length representation of a section of three conductors line.

three-conductors line section of length Δx, where r_i, l_k, g_k, c_k with $i \in \{0,\ 1,\ 2\}$ and $k \in \{1,\ 2\}$ denote the p.u.l. resistance, inductance, conductance and capacitance, respectively. The p.u.l. inductance l_m, the conductance g_m and the capacitance c_m take into account for the mutual interactions between conductors. With three wires, two different circuits sharing the same return conductor are given. Clearly, the two circuits are coupled. Note also that we neglect the leakage currents towards the physical earth, therefore the current is supposed to flow only through the phase, neutral and PE conductors. We assume the neutral to be the reference conductor, thus we define the circuit 1 as the one between the phase and the neutral wires, and the circuit 2 as the one between the ground and the neutral wires.

Now, let us denote with $V_k(f,x)$ and $I_k(f,x)$, for $k \in \{1,\ 2\}$, the voltage and the current phasors associated to the two circuits at frequency f and coordinate x. By letting $\Delta x \to 0$ in Fig. 1, we obtain the telegraph equations

$$\frac{\partial \mathbf{V}(f,x)}{\partial x} = -\big(\mathbf{R} + j2\pi f\mathbf{L}\big)\mathbf{I}(f,x)\,, \tag{1}$$

$$\frac{\partial \mathbf{I}(f,x)}{\partial x} = -\big(\mathbf{G} + j2\pi f\mathbf{C}\big)\mathbf{V}(f,x)\,, \tag{2}$$

where, $\mathbf{V}(f,x) = [V_1(f,x),\ V_2(f,x)]^T$ is the voltage phasor vector, $\mathbf{I} = [I_1(f,x),\ I_2(f,x)]^T$ is the current phasor vector, and

$$\mathbf{R} = \begin{bmatrix} r_1 + r_0 & r_0 \\ r_0 & r_2 + r_0 \end{bmatrix}\,, \quad \mathbf{L} = \begin{bmatrix} l_1 & l_m \\ l_m & l_2 \end{bmatrix}\,,$$

$$\mathbf{C} = \begin{bmatrix} c_1 + c_m & -c_m \\ -c_m & c_2 + c_m \end{bmatrix}\,, \quad \mathbf{G} = \begin{bmatrix} g_1 + g_m & -g_m \\ -g_m & g_2 + g_m \end{bmatrix}\,,$$

are the p.u.l. parameter matrices for the resistance, inductance, capacitance and conductance, respectively. We use the $\{\cdot\}^T$ to denote the transposition and we do not explicitly show the frequency dependency in the following.

We further define the impedance matrix $\mathbf{Z}$, the admittance matrix $\mathbf{Y}$ and the eigenvalue decomposition of their product as

$$\mathbf{Z} = \mathbf{R} + j\omega\mathbf{L}\,, \tag{3}$$

$$\mathbf{Y} = \mathbf{G} + j\omega\mathbf{C}\,, \tag{4}$$

$$\mathbf{YZ} = \mathbf{T}\mathbf{\Lambda}\mathbf{T}^{-1}\,, \tag{5}$$

respectively, where $\mathbf{T}$ is the eigenvector matrix and $\mathbf{\Lambda} = diag\{\lambda_1,\ \lambda_2\}$ is the eigenvalue matrix. Now, if we define the modal current $\mathbf{I}_m = \mathbf{T}^{-1}\mathbf{I}$, we can exploit the telegraph equations to obtain

$$\mathbf{I}(x) = \mathbf{T}\mathbf{I}_m = \mathbf{T}\Big(\mathbf{e}^{-\mathbf{\Gamma}x}\mathbf{I}_m^+ + \mathbf{e}^{\mathbf{\Gamma}x}\mathbf{I}_m^-\Big)\,, \tag{6}$$

$$\mathbf{V}(x) = \mathbf{Y}^{-1}\mathbf{T}\mathbf{\Gamma}\Big(\mathbf{e}^{-\mathbf{\Gamma}x}\mathbf{I}_m^+ - \mathbf{e}^{\mathbf{\Gamma}x}\mathbf{I}_m^-\Big)\,, \tag{7}$$

where $\mathbf{\Gamma} = diag\{\gamma_1, \gamma_2\}$ is such that $\mathbf{\Gamma\Gamma} = \mathbf{\Lambda}$, $\mathbf{e}^{\pm\mathbf{\Gamma}x} = diag\{e^{\pm\gamma_1 x}, e^{\pm\gamma_2 x}\}$ and $\mathbf{I}_m^+$, $\mathbf{I}_m^-$ are vectors whose coefficients are determined from the boundary conditions. The result is a modal expression for both the voltage and the current phasor vectors. Note that the voltages and the currents maintain the same structure of the two-conductor line case.

Starting from (6)-(7), we can also define the characteristic impedance of the multiconductor transmission line as the matrix $\mathbf{Z}_C = \mathbf{Y}^{-1}\mathbf{T}\mathbf{\Gamma}\mathbf{T}^{-1}$. Furthermore, we introduce the load reflection coefficient matrix $\boldsymbol{\rho}_{L_I}$ such that $\mathbf{I}_m^- = \boldsymbol{\rho}_{L_I}\mathbf{I}_m^+$, where we use the subscript I in the notation to highlight the fact that $\boldsymbol{\rho}_{L_I}$ relates current quantities. Then, by letting $x = 0$ at the end of the multiconductor line, we obtain

$$\boldsymbol{\rho}_{L_I} = \mathbf{T}^{-1}\mathbf{Z}_C^{-1}\big(\mathbf{Y}_L + \mathbf{Y}_C\big)^{-1}\big(\mathbf{Y}_L - \mathbf{Y}_C\big)\mathbf{Z}_C\mathbf{T}\,, \tag{8}$$

where $\mathbf{Y}_C = \mathbf{Z}_C^{-1}$, and $\mathbf{Y}_L$ is the equivalent admittance matrix of the load connected at the end of the line, i.e., by definition, $\mathbf{I}(0) = \mathbf{Y}_L\mathbf{V}(0)$.

Now, combining (6)-(7) and (8), we can determine the admittance matrix $\mathbf{Y}_R(x)$ at coordinate x as the matrix that satisfies the relation $\mathbf{I}(x) = \mathbf{Y}_R(x)\mathbf{V}(x)$. Furthermore, $\mathbf{Y}_R(x)$ can be also interpreted as the load admittance carried back at coordinate x. Strictly,

$$\mathbf{Y}_R(x) = \mathbf{T}\big(\mathbf{e}^{-\mathbf{\Gamma}x} + \mathbf{e}^{\mathbf{\Gamma}x}\boldsymbol{\rho}_{L_I}\big) \times \big(\mathbf{e}^{-\mathbf{\Gamma}x} - \mathbf{e}^{\mathbf{\Gamma}x}\boldsymbol{\rho}_{L_I}\big)^{-1}\mathbf{T}^{-1}\mathbf{Y_C}\,. \tag{9}$$

This final relation is of key importance for the multiconductor extension of the voltage ratio approach method that will be described in the next section.

B. MTL Extension of the Voltage Ratio Approach

In [9] we devised an efficient algorithm for the CTF computation in complex networks that can be easily extended to the MTL scenario as follows.

We firstly remap the topology. We find the backbone, i.e., the shortest signal path between the transmitter and the receiver. Then, we model the rest of the network as branches connected to the nodes of the backbone. Finally, we split the backbone into small elements called units. A unit contains a piece of backbone line, a backbone node and the branches connected to the backbone node.

We compute the CTF as the product of the MTL insertion loss of each unit. Fig. 2 shows an unifilar representation of an MTL remapped topology on the top, and the correspondent representation in units on the bottom. The coordinates on the x axis refer to the position of the backbone nodes. We use thick lines to represent the uniform pieces of backbone. Each unit $b \in \{1, \ldots, N\}$ contains the branches connected to the backbone node n_b, and the uniform piece of backbone line

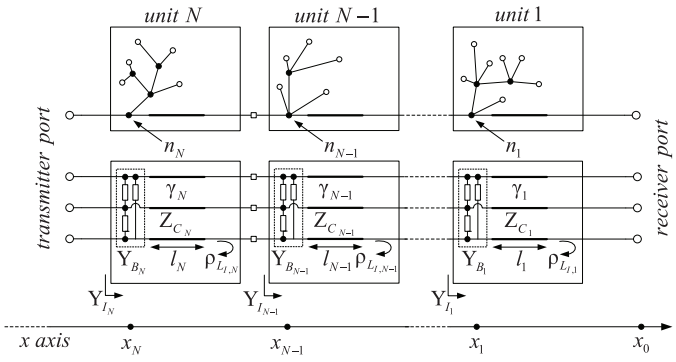

Fig. 2. On the top, unifilar description of the remapped topology. On the bottom, the correspondent representation in units.

between nodes n_b and n_{b-1}, where n_0 is the receiver node. We refer to $\mathbf{Z}_{C_b}$, $\boldsymbol{\gamma}_b$ and l_b as the characteristic impedance, the propagation constant and the length of the piece of backbone line that belongs to unit b, respectively. Furthermore, we represent multiple branches that depart from the backbone node n_b as an equivalent admittance, whose matrix $\mathbf{Y}_{B_b}$ is obtained by carrying back the terminal loads of the branch up to the backbone node n_b, according to (9). We also compute the reflection coefficient matrix of each unit b, i.e., $\boldsymbol{\rho}_{L_{I,b}}$. To this aim, we exploit (8), where we substitute $\mathbf{Z}_C$ and $\mathbf{Y}_L$ with the characteristic impedance $\mathbf{Z}_{C_b}$ and the load admittance matrix of unit b, respectively. The latter represents the admittance seen from the port towards the receiver of unit b, namely $\mathbf{Y}_{I_{b-1}}$. If $b = 1$, $\mathbf{Y}_{I_{b-1}}$ is the receiver admittance matrix. Now, for each unit b, the correspondent reflection coefficient matrix $\boldsymbol{\rho}_{L_{I,b}}$ can be used to provide the relation between the voltages at the ends of the unit, i.e., the MTL voltage insertion loss. According to the notation of Fig. 2, by introducing the reflection coefficient matrix into (7) it follows that

$$\begin{aligned}\mathbf{V}(x_b) = \mathbf{Z}_{C_b}\mathbf{T}_b\big(\mathbf{e}^{\gamma l_b} - \mathbf{e}^{-\gamma l_b}\boldsymbol{\rho}_{L_I,b}\big) \\ \times \big(\mathbf{U} - \boldsymbol{\rho}_{L_I,b}\big)^{-1}\mathbf{T}_b^{-1}\mathbf{Z}_{C_b}^{-1}\mathbf{V}(x_{b-1})\,, \quad (10)\end{aligned}$$

where $\mathbf{U}$ is the identity matrix of dimension 2×2 and $\mathbf{T}_b$ is the eigenvector matrix associated to the uniform piece of backbone line of unit b. Now, the voltage insertion loss of unit b is defined as the matrix $\mathbf{H}_b(f)$ such that

$$\mathbf{V}(f, x_{b-1}) = \mathbf{H}_b(f)\mathbf{V}(f, x_b)\,, \quad (11)$$

where we highlight the frequency dependence that we have previously omitted to simplify the notation. Therefore, the voltage insertion loss $\mathbf{H}_b(f)$ can be immediately obtained from (10) by means of inversion. Furthermore, since the overall MTL insertion loss $\mathbf{H}(f)$ is such that $\mathbf{V}(f, x_0) = \mathbf{H}(f)\mathbf{V}(f, x_N)$, it can be computed as follows

$$\mathbf{H}(f) = \prod_{b=1}^{N} \mathbf{H}_b(f)\,, \quad (12)$$

that is, the product of the voltage insertion loss of all the units. Note that the product has to be computed starting from the insertion loss of the unit close to the receiver. We also point out that the MTL insertion loss matrix $\mathbf{H}(f)$ is the channel transfer function matrix of the MIMO transmission scheme, namely $\mathbf{H}_{MIMO}(f) = \mathbf{H}(f)$. We further denote with $H_{MIMO,ik}(f)$ the element of the i-th row and k-th column of the matrix $\mathbf{H}_{MIMO}(f)$, i.e., the channel transfer function between the transmitter connected to the i-th circuit and the receiver connected to the k-th circuit, where $i, k \in \{1, 2\}$.

An interesting subcase of the MIMO transmission scheme is the SIMO configuration. In this case, we transmit only on a circuit, without any loss of generality the circuit 1, and we receive on both the circuits. It follows that $\mathbf{V}(f, 0) = \mathbf{H}_{SIMO}(f)V_1(f, x_N)$. Therefore, we switch off the transmitter placed on circuit 2 and we assume the circuit 2 to be closed into a $50\,\Omega$ impedance at both the transmitter and the receiver end. Now, we define $\mathbf{Y}_I(f)$ as the input admittance matrix of unit N. Then, the resultant SIMO insertion loss is given by

$$\mathbf{H}_{SIMO}(f) = \mathbf{H}_{MIMO}(f)\boldsymbol{\alpha}(f) \quad (13)$$

where $\boldsymbol{\alpha}(f) = [1 - Y_{21,I}(f)/(Y_{22,I}(f) + 1/50)]^T$ takes into account for the SIMO boundary conditions at the transmitter side, and $Y_{ik,I}$ denotes the element of the i-th row and k-th column of the matrix $\mathbf{Y}_I(f)$.

III. Random Generator

We now provide the statistical model of in-home PLC networks. We investigate the arrangement of the outlets, the interconnections of the cables, and the distribution of the loads.

A. The Topology Generation Algorithm

We focus on single-phase PLC in-home networks for which in [8] we have provided a topology model based on regulations and commons practices. We recall it here for the sake of completeness. Basically, we have found that in-home networks are made of two levels of connections. At a first layer, outlets are connected in groups to special nodes, that we refer to as derivation boxes. Then, at a second layer, the derivation boxes are connected together with dedicated cables. We have observed that the outlets fed by the same derivation box are nearby placed and the derivation boxes are almost regularly spaced inside the topology. Therefore, we split the topology into area elements each of which contains all the outlets connected to a derivation box and the derivation box itself. We refer to these area elements as clusters. We model the clusters as square-shaped elements and we assume their area A_c constant for a specific topology realization and uniformly distributed in a realistic interval. It follows that the number of cluster for a given topology of area A_f is $\lceil A_f/A_c \rceil$. We model the topology area A_f as a uniform distributed random variable and the number of outlets in each cluster as a Poisson variable with mean $\Lambda_o A_c$, where Λ_o is the number of $\mathrm{outlets/m^2}$. Clusters are interconnected via derivation boxes and the in-home network is connected to the energy supplier network via the main panel. In some countries, as for instance the United States, the neutral wire and the PE wire are short circuited in the main panel. We refer to this particular configuration

TABLE I
PARAMETER SET FOR THE BOTTOM-UP GENERATOR

Parameter	Value
$A_f\ (m^2)$	$\mathcal{U}(100, 300)$
$\Lambda_o\ (outlets/m^2)$	0.5
$A_c\ (m^2)$	$\mathcal{U}(15, 45)$
p_v	0.3

as short circuited-main panel (SC-MP). Otherwise, when the neutral and the PE wires are not short circuited, we refer to the configuration as standard.

We model the interconnections as multiconductor transmission lines where the three wires are nearby placed and enclosed in a uniform dielectric cap. The conductor inter-distance is further assumed to be constant.

The effect of loads has also been considered. We randomly generate a set of 50 loads and we define p_v as the probability that no loads are connected to a plug. Then, the probability that a load extracted from this set is connected to a plug is given by $\big(1 - p_v\big)/50$.

In Table I, we report the set of values for all the parameters required by the topology generation algorithm. $\mathcal{U}(a, b)$ denotes a uniform distributed random variable in the interval $(a,\ b)$. More details can be found in [11].

B. Statistical Load Distribution

Electrical appliances connected to the network significantly affect the PLC CTF. Thus, we have studied their characterization in order to fit the reality as much as possible. We model the loads in terms of admittance matrices, i.e., we relate the currents and the voltages at the input ports of the loads as $\mathbf{I} = \mathbf{YV}$, where $\mathbf{Y}$ is the admittance matrix representation of the load.

Starting from an exhaustive measurement campaign, we have collected the input impedances of several in-home appliances. Then, we have derived a statistical in-home load impedance generator for the three conductor system. Results are not herein reported for space limitations.

IV. CHANNEL STATISTICS

In this work we mainly focus on the statistics of the channel capacity. We study the performances of the 2×2 MIMO PLC and the 1×2 SIMO PLC. In this latter case, we both consider the maximum ratio combining (MRC) and the selection diversity (SD) scheme. Results are then compared to the ones of the SISO transmission scheme.

A. MIMO Channel Capacity

We initially consider a 2×2 MIMO PLC system, where the signal is both transmitted and received on the two circuits. We consider a multicarrier modulation system with N sub-channels defined in the band $B = [B_1, B_2]$. Therefore, $W = B/N$ is the sub-channel bandwidth. We suppose the channel to be approximately flat and time invariant for each sub-channel. According to the notation of Section II-A, we define $H_{ik,n} = H_{MIMO,ik}(f)$ as the channel transfer function for the n-th sub-channel when the transmitter is connected to the i-th circuit and the receiver is connected to the k-th circuit, where $i, k \in \{1, 2\}$, $n = 1, \ldots, N$, and $f = W(n-1) + B_1$. Again, $H_{ik,n}$ denotes the element of the i-th row k-th column of the matrix $\mathbf{H}_n$. Concerning the noise, we model it as colored Gaussian background noise with a power spectral density $P_w(f)$ that is equal for the two circuits and approximately constant in the n-th sub-channel, namely $P_{w,n} = P_w(f)$,where $f = (n-1)W + B_1$. We further assume the different circuits to experience uncorrelated noise.

In order to compare the results with the experimental ones [7], we fix the total transmitted power and we assume the channel to be unknown at the transmitter. It follows that, in 2×2 MIMO PLC, we transmit on both circuits with the same power spectral density $P_t(f)/2$. We approximate $P_t(f)$ as constant on the n-th sub-channel, i.e., $P_{t,n} = P_t(f)$, $f = (n-1)W + B_1$. Therefore, by letting $\gamma_n = P_{t,n}/P_{w,n}$, it follows that

$$C_{MIMO} = W \sum_{n=1}^{N} \log_2 \left[\det\Big(\mathbf{U} + \mathbf{H}_n \mathbf{H}_n^H \frac{\gamma_n}{2} \Big) \right], \qquad (14)$$

where $\mathbf{U}$ is the 2×2 identity matrix. $\{\cdot\}^H$ denotes the hermitian transpose. Now, let us introduce the eigenvalue decomposition of the matrix $\mathbf{H}_n \mathbf{H}_n^H$

$$\mathbf{H}_n \mathbf{H}_n^H = \mathbf{A}_n \mathbf{\Phi}_n \mathbf{A}_n^H\ , \qquad (15)$$

where $\mathbf{A}_n$ is the unitary eigenvector matrix and $\mathbf{\Phi}_n = diag\{\phi_{1,n}, \phi_{2,n}\}$ is the eigenvalue matrix. Then, the MIMO capacity under the Gaussian noise assumption can be written as [12]

$$C_{MIMO} = W \sum_{n=1}^{N} \sum_{i=1}^{2} \log_2 \left(1 + \phi_{i,n} \frac{\gamma_n}{2} \right), \qquad (16)$$

where $\phi_{i,n}$ are the eigenvalues of the matrix $\mathbf{H}_n \mathbf{H}_n^H$.

B. SIMO Channel Capacity

The full 2×2 MIMO PLC scheme requires two transmitters and two receivers. Another interesting configuration is the 1×2 SIMO configuration, that requires only one transmitter and two receivers. We evaluate the SIMO capacity under the same conditions of noise reported in Section IV-A. We both consider the MRC and SD schemes. Firstly, we define the channel transfer function matrix for the SIMO case. Since only one transmitter is present, the CTF in the SIMO case is a vector of two elements that are equal to $H_{i,n} = H_{SIMO,i}(f)$ where $f = W(n-1) + B_1$, and we refer to $H_{1,n}$ and $H_{2,n}$ as the direct link and the coupled link, respectively. In the MRC scheme the receiver collects the signals received on different circuits and linearly combines them exploiting the spatial diversity. Therefore, from (14) the capacity of the MRC SIMO scheme is equal to [12]

$$C_{SIMO,MRC} = W \sum_{n=1}^{N} \log_2 \left(1 + \sum_{i=1}^{2} |H_{i,n}|^2 \gamma_n \right). \qquad (17)$$

Conversely, in the selection diversity scheme the receiver chooses the best signal received on different circuits. It follows that the SD SIMO capacity is given by

$$C_{SIMO,SD} = \max_i \left(W \sum_{n=1}^{N} \log_2 \left(1 + |H_{i,n}|^2 \gamma_n \right) \right) \quad (18)$$

As also reported [7], we have found that the direct link does not necessarily outperform the coupled link.

C. SISO Channel Capacity

In the SISO case, one transmitter and one receiver are used and both are connected to the same circuit. Without any loss of generality, we transmit and receive on the circuit 1, namely between the phase and neutral wire. We further assume both the ends of the second circuit closed into a $50\,\Omega$ impedance, as done for the SIMO configuration. Therefore, the channel capacity in the SISO case is given by

$$C_{SISO} = W \sum_{n=1}^{N} \log_2 \left(1 + |H_{1,n}|^2 \gamma_n \right), \quad (19)$$

where $H_{1,n}$ is the SIMO channel response for the n-th sub-channel when both the transmitter and the receiver are connected to the same circuit, namely, circuit 1.

V. Numerical Analysis Results

We herein combine the topology generation algorithm and the MTL extension of the voltage ratio approach to generate MIMO PLC channel transfer functions and then, we compute their MIMO capacity and correlation. A set of 1000 channel realizations have been considered. We will show that the results are statistically in good agreement with reality. Furthermore, we infer the capacity of the SIMO configuration and we compare the results with the SISO case. Finally, we study the capacity improvements given by the deployment of multiple transmitters and receivers in topologies where the neutral and the PE wires are short circuited in the main panel.

We focus on the 2-100 MHz band and we assume the sub-channel band equal to $W = 50$ kHz. Therefore, $N = 1961$ sub-channels have been considered. We transmit according to a fixed PSD mask, that is, -50 dBm/Hz up to 30 MHz, and -80 dBm/Hz otherwise. The analytical expression of the colored background noise PSD is given by

$$P_w(f) = 10 \log_{10} \left(\frac{1}{f^2} + 10^{-15.5} \right) [dBm/Hz], \quad (20)$$

which is the result of the experimental measurement campaign in [13].

A. Capacity Improvement in Standard Networks

We carry out a statistical analysis of the capacity for the MIMO, the MRC-SIMO, the SD-SIMO and the SISO configurations in standard networks. In Fig. 3a we provide the results in terms of complementary cumulative distribution function (CCDF), while in Table II we provide the maximum, mean and minimum value of capacity for all the configurations. As

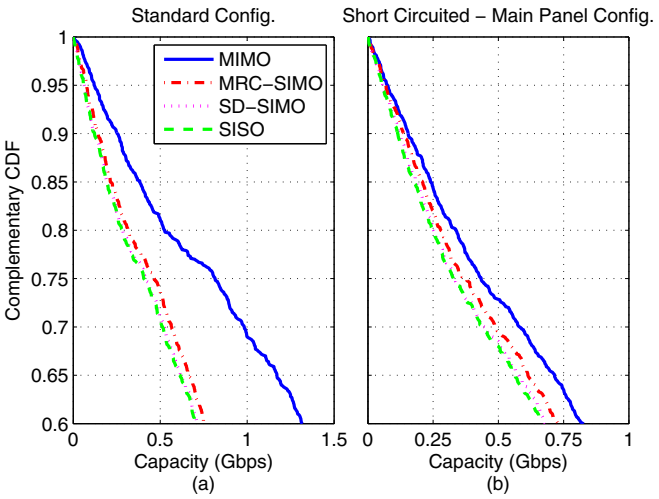

Fig. 3. Complementary cumulative distribution function of the capacity for different schemes in (a) the standard networks, (b) the SC-MP networks.

TABLE II
Minimum, mean and maximum values for MIMO capacity

Network Config.	MIMO Capacity Min (Mbps)	Mean (Gbps)	Max (Gbps)
Standard	809	1.719	4.768
SC-MP	3.127	1.359	4.586

can be noted, the MIMO scheme clearly outperforms the other solutions. In particular, if we define the capacity ratios

$$\eta_{MIMO} = C_{MIMO}/C_{SISO}\,, \quad (21)$$

$$\eta_{SIMO,MRC} = C_{SIMO,MRC}/C_{SISO}\,, \quad (22)$$

$$\eta_{SIMO,SD} = C_{SIMO,SD}/C_{SISO}\,, \quad (23)$$

we find that, on average, the SIMO capacity ratios are close to 1, namely, $\eta_{SIMO,MRC} = 1.13$ and $\eta_{SIMO,SD} = 1.05$, while the MIMO capacity ratio η_{MIMO} is approximately 2. We point out that this result is in good agreement with the one reported in [7]. MRC-SIMO and SD-SIMO improvements are lower w.r.t. to the MIMO one. Nevertheless, we point out that while the MIMO scheme requires two transmitters and receivers, the SIMO configurations can be implemented by simply adding a second receiver to the SISO configuration.

B. Channel Correlation Analysis

Herein, we focus on the correlation among MIMO PLC channels. To this aim, we firstly study the sub-channel correlation coefficient R_n, that is defined as [7]

$$R_n = \frac{\max_i \{\phi_{i,n}\}}{\sum_{i=1}^{2} \phi_{i,n}}\,, \quad (24)$$

where we refer to the notation presented in Section IV-A. Then, we average R_n over the sub-channels to obtain the

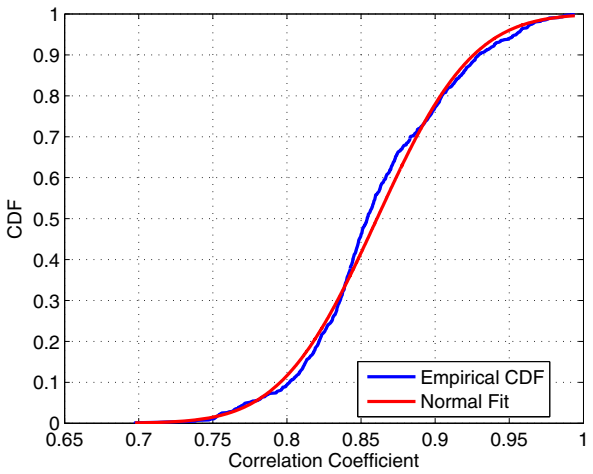

Fig. 4. Cumulative distribution function of the correlation coefficient R, and its normal fit.

correlation coefficient

$$R = \frac{1}{N}\sum_{n=1}^{N} R_n \, . \tag{25}$$

The correlation coefficient R is a scalar quantity defined between 0.5 and 1. Strictly, as the correlation coefficient approaches 1, the two MIMO PLC channels become perfectly correlated. In Fig. 4, we report the cumulative distribution function (CDF) of the coefficient and its normal fit. More in detail, we have found that the normal distribution with mean 0.8608 and variance 0.0509 is the best fit for R. As it can be noted, R assumes values close to 1 with high probability, therefore MIMO PLC channels show a high correlation coefficient. We note that these results are consistent with the experimental ones provided in [7].

C. Capacity Improvement in SC-MP Networks

In this section we focus on the capacity improvement given by the MIMO scheme in short circuited main panel networks. As specified by the NEC, in SC-MP networks the neutral wire and the PE wire are short circuited in the main panel. This means that the signal transmitted on the circuit 2 cannot be directly received on the same circuit when the link goes across the main panel. Anyhow, not all the links are supposed to cross the main panel and further, if so, the MIMO schemes can still yield a capacity improvement. Therefore, we study 1000 channel realizations extracted from SC-MP networks where the transmitter and receiver outlets are randomly picked. We compare the MIMO, the MRC-SIMO and the SD-SIMO capacity to the SISO one. We provide the resultant CCDFs in Fig. 3b and the maximum, mean and minimum values of capacity in Table II. The MIMO scheme still performs better, although the capacity improvement is clearly lower than the one observed in Section V-A. Strictly, for the SC-MP networks we have found that $\eta_{MIMO} = 1.545$, $\eta_{SIMO,MRC} = 1.104$ and $\eta_{SIMO,SD} = 1.028$.

VI. Conclusion

We have presented a statistical bottom-up MIMO PLC random channel generator. It is based on a random topology generation algorithm and on the multiconductor extension of the voltage ratio approach presented in [9].

We have exploited the channel generator to infer the statistics of the channel capacity when the MIMO, the maximal ratio combining and the selection diversity SIMO configurations are deployed. For the MIMO scheme, we have compared the results with the experimental ones and we have found that the simulated MIMO capacity is consistent, on average, to the experimental one. Furthermore, we have investigated the correlation among MIMO channels. Again, we have found that, on average, simulated channels present a correlation that is in good agreement with the experimental one. Finally, we have studied the capacity improvement given by MIMO schemes in topologies where the neutral and the protective earth wires are short circuited in the main panel. We have found that in this case gains are still obtained.

References

[1] Home plug alliance. [Online]. Available: www.homeplug.org
[2] A. M. Tonello, P. Siohan, A. Zeddam, and X. Mongaboure, "Challenges for 1 Gbps power line communications in home networks," in *proc. IEEE Int. Symp. Personal, Indoor and Mobile Radio Commun. (PIMRC)*, Sep. 2008, pp. 1–6.
[3] G. J. Foschini and M. J. Gans, "On Limits of Wireless Communications in a Fading Environment when Using Multiple Antennas," *Wireless Personal Communications*, vol. 6, no. 3, pp. 311–335, Mar. 1998.
[4] C. L. Giovaneli, P. G. Farrell, and B. Honary, "Improved Space-Time Coding Applications for Power Line Channels," in *Proc. IEEE Int. Symp. Power Line Commun. and its App. (ISPLC)*, Mar. 2003, pp. 50–55.
[5] C. L. Giovaneli, B. Honary, and P. G. Farrell, "Space-Frequency Coded OFDM System for Multi-Wire Power Line Communications," in *Proc. IEEE Int. Symp. Power Line Commun. and its App. (ISPLC)*, Apr. 2005, pp. 191–195.
[6] L. Stadelmeier, D. Schill, D. Schneider, and J. Speidel, "Precoded Spatial Multiplexing MIMO for Inhome Power Line Communications," in *Proc. IEEE Global Communications Conference (GLOBECOM)*, Dec. 2008, pp. 1–5.
[7] R. Hashmat, P. Pagani, A. Zeddam, and T. Chonavel, "MIMO Communications for Inhome PLC Networks: Measurements and Results up to 100 MHz," in *Proc. IEEE Int. Symp. Power Line Commun. and its App. (ISPLC)*, Apr. 2010.
[8] A. M. Tonello and F. Versolatto, "Bottom-Up Statistical PLC Channel Modeling - Part I: Random Topology Model and Efficient Transfer Function Computation," *to appear in IEEE Trans. on Power Del.*, 2011.
[9] A. M. Tonello and T. Zheng, "Bottom-Up Transfer Function Generator for Broadband PLC Statistical Channel Modeling," in *Proc. IEEE Int. Symp. Power Line Commun. and its App. (ISPLC)*, Apr. 2009.
[10] R. P. Clayton, *Introduction to Electromagnetic Compatibility*, second edition ed. New Jersey: Wiley & Sons, 2006.
[11] A. M. Tonello and F. Versolatto, "Bottom-Up Statistical PLC Channel Modeling - Part II: Inferring the Statistics," *IEEE Trans. on Power Del.*, vol. 25, no. 4, pp. 2356–2363, Oct. 2010.
[12] B. Vucetic and J. Yuan, *Space - Time Coding*. John Wiley & Sons, 2003.
[13] F.P.7 Theme 3 ICT-213311 OMEGA, "PLC Channel Characterization and Modelling," Deliverable 3.2, Dec. 2008.